Chemical Engineering Journal 445 (2022) 136530

Contents lists available at ScienceDirect

Chemical Engineering Journal

journal homepage: www.elsevier.com/locate/cej

Cerium manganese oxides coupled with ZSM-5: A novel SCR catalyst with superior K resistance

Jiawei Ji [a], Yu Tang [a], Li Han [a], Pan Ran [a], Wang Song [a], Yandi Cai [b], Wei Tan [a], Jingfang Sun [d], Changjin Tang [c,*], Lin Dong [a,b,d,*]

[a] Laboratory of Mesoscopic Chemistry of MOE, School of Chemistry and Chemical Engineering, Nanjing University, Nanjing 210023, PR China
[b] School of the Environment, Nanjing University, Nanjing 210023, PR China
[c] School of Environment, Nanjing Normal University, Nanjing 210023, PR China
[d] Jiangsu Key Laboratory of Vehicle Emission Control, Center of Modern Analysis, Nanjing University, Nanjing 210023, PR China

ARTICLE INFO

Keywords:
CeMn mixed oxides
ZSM-5 hybridization
NH_3-SCR
K resistance
Deactivation mechanism

ABSTRACT

The application of cerium-manganese oxides (CeMn) in controlling exhaust gas from biomass combustion is greatly inhibited due to poor resistance to alkali metals. Herein, we report a smart strategy to circumvent the K poisoning problem of CeMn by physically coupling with ZSM-5, which exhibited almost no activity loss even under a high loading of 2 *wt*% K_2O. Results showed that in contrast to the conventionally believed disturbance of redox property and reduction of acid sites, the dominant effect from K loading on the deactivation of CeMn catalysts lies on the formation of chemically inert nitrates, which significantly restrains the reaction cycle via Langmuir-Hinshelwood route. With ZSM-5 hybridization, the stable nitrates over CeMn can be facilely activated and consumed by NH_4^+ species introduced by ZSM-5, thus transforming poisoning sites into active sites and ensuring superior catalytic performance. The study presenting here not only provides an efficient strategy for fabricating NH_3-SCR catalysts with superior K resistance but also sheds new light on the deactivation mechanism of K over CeMn catalysts.

1. Introduction

Nitrogen oxides (NO_x, composed of NO and NO_2) emitted from stationary and mobile sources are severe atmospheric pollutants inducing ozone destruction, photochemical pollution, and acid rain. Selective catalytic reduction of NO by NH_3 (NH_3-SCR) is currently the most popular and efficient method in governing NO_x emission from stationary sources. As one of the most successful commercial catalysts, V_2O_5-WO_3/TiO_2 is widely employed in controlling NO_x from thermal power plants, which shows excellent medium–high temperature activity, good selectivity, and SO_2/H_2O resistance [1–3]. However, along with the increased environmental awareness and demanding need for renewable energy, the employment of biomass resources with low carbon emission features is encouraged to replace fossil energy for power generation in thermal plants. Traditional V_2O_5-WO_3/TiO_2 can hardly meet these emerging demands due to the harsh working condition of low temperature (< 200 °C) and high content of alkali metals. Potassium (K), sodium (Na), and some other alkali metals in biomass burning can result in continuous and irreversible deactivation of SCR catalysts [4–6]. Thus, it is of significant importance to design catalysts with high low-temperature activity and superior alkali metal resistance.

Alkali metals in fly ash are usually thought to result in decrease of reducibility and loss of surface acidity [7–9]. Li *et al.* found the SCR activity of V_2O_5-WO_3/TiO_2 sharply declined from 100% to less than 25% even with 1 *wt*% Na loading. The presence of Na can not only occupy acidic sites but also interact with active V species, resulting in decreased V^{5+} species and disturbed reducibility [10]. Accordingly, the current anti-alkali metal strategies mainly include creating more surface acid sites and constructing capture sites to protect active sites. Tang *et al.* proposed a dual-site mechanism of HMO (hollandite manganese oxide) to promote K resistance. The sites on the external surface act as catalytic active, while sites in the internal tunnels can capture alkali metal ions and protect the external surface from being poisoned [11]. Yao *et al.* used a simple H_2SO_4 pretreatment to obtain acid-pretreated CeO_2-TiO_2/P25, which exhibited great improvement in anti-alkali metal compared with the original catalyst [6]. Zhang *et al.* prepared a hollandite Mn-Ti

* Corresponding authors at: Laboratory of Mesoscopic Chemistry of MOE, School of Chemistry and Chemical Engineering, Nanjing University, Nanjing 210023, PR China (L. Dong). School of Environment, Nanjing Normal University, Nanjing 210023, PR China (C. Tang).
E-mail addresses: tangcj@njnu.edu.cn (C. Tang), donglin@nju.edu.cn (L. Dong).

https://doi.org/10.1016/j.cej.2022.136530
Received 26 January 2022; Received in revised form 27 March 2022; Accepted 19 April 2022
Available online 22 April 2022

oxides-protected Cu-SAPO-34 catalysts with good resistance to alkali metals poisoning. The Mn-Ti oxides acted as sacrifice sites to prevent Cu-SAPO-34 from being poisoned by alkali metal ions [12].

Mn-based catalysts are considered as one of the most efficient low-temperature (< 200 °C) denitrification catalysts because of their superior redox property and abundant acid sites. Quite a lot of Mn-based materials such as MnTi, MnAl, MnSn, and CeMn have been investigated [13–16]. Among them, CeMn catalysts have been regarded as the most promising one due to their dramatic low-temperature activity for NO_x removal (yields nearly 100% NO conversion at 100-150 °C with a space velocity of 42,000 h^{-1}) [17]. Unfortunately, they still suffer from heavy deactivation in the presence of alkali metals [18].

Herein, a hybridization strategy was reported for the first time to obtain CeMn catalysts with superior resistance to K. We found that the cut-off of Langmuir-Hinshelwood (L-H) mechanism from K induced inert nitrates was the main reason for CeMn deactivation and the resistance can be greatly enhanced by simply coupling with ZSM-5 through mechanical grinding. Kinetics study, transient experiment, *in situ* DRIFTS, and TPD of surface species were jointly employed to investigate the deactivation mechanism of CeMn catalyst and the essential role of ZSM-5 in activating inert nitrates and regenerating poisoned catalysts was confirmed.

2. Materials and methods

2.1. Preparation of catalysts

CeMn mixed oxides were obtained by the conventional co-precipitation method. Calculated quantity of $(NH_4)_2Ce(NO_3)_6$ (0.0217 mol) and $Mn(NO_3)_2{\cdot}9H_2O$ (0.0145 mol) were dissolved in 150 mL distilled water under stirring. Then, $NH_3{\cdot}H_2O$ (25%) was dropped into the mixed solution slowly until the pH value reached 10. The obtained solution was aged for 10 h, filtered, and washed with distilled water for several times. The resulting solid was dried in the oven at 110 °C overnight and then calcined in the muffle furnace at 500 °C for 4 h (the ramping rate was 2 °C/min). The sample was marked as CeMn. ZSM-5 (Si/Al = 12.5) was directly purchased from Zhuoran Environmental Production (Dalian) Co., Ltd. The hybrid catalyst was prepared by grinding 1 g ZSM-5 and 1 g CeMn in an agate mortar for 0.5 h and was labeled as CeMn-Z5.

K was chosen to investigate the anti-alkali poisoning ability of CeMn and hybrid catalysts. Different ratios of K_2O (0.5%, 1%, and 2% in weight) poisoned catalysts were prepared through an impregnation method. In a typical process, 0.0428 g KNO_3 was dissolved in 30 mL deionized water and magnetically stirred for 30 min. Then 1 g CeMn was dropped into the solution and stirred for 1 h. After evaporation of excessive water at 100 °C in an oil bath, the sample was transferred to an oven and dried under 100 °C overnight followed by air calcination in a muffle under 400 °C for 4 h with a ramping rate of 2 °C/min. The sample was labeled as 2K/CeMn. The other samples were also named as xK/CeMn or xK/CeMn-Z5 (x = 0.5, 1, or 2) according to the nominal loadings.

2.2. Catalyst characterization

The specific surface area was characterized by the N_2-sorption technique at -196 °C on Micromeritics ASAP-2020 adsorption apparatus. All samples were vacuum-pretreated at 300 °C for 3 h before measurement.

X-ray powder diffraction (XRD) patterns were collected on a Philips X'pert Pro diffractometer with Ni-filtered Cu Kα radiation (0.15408 nm). The scan range is from 20.0 to 60.0° with a scan speed of 10.0°/min. The sampling pitch is 0.02°.

X-ray photoelectron spectroscopy (XPS) measurements were conducted using a PHI 5000 Versa Probe system with a monochromatic Al Kα radiation (1486.6 eV, 15 kW). All binding energies were calibrated by the adventitious C *1s* (284.8 eV) to compensate for surface charge effects.

Transmission electron microscopy (TEM) images were taken on a JEM-1011 instrument at an acceleration voltage of 200 kV.

Scanning electron microscopy (SEM) images were collected on a Philips XL30 electron microscope (10.0 kV). The EDS-mapping images were performed on a FEI Tecnai G2 F20 transmission electron microscope operating at 200 kV.

STEM images were obtained using a high-angle annular dark-field detector (HAADF). All samples were dispersed in A.R. grade ethanol with ultrasonic treatment for 1 h and the resulting suspension was allowed to dry on a carbon film supported on copper grids.

Temperature-programmed reduction by H_2 (H_2-TPR) was carried out in a quartz U-tube reactor connected to a thermal conduct detector (TCD) with the H_2/Ar mixture (7% H_2 by volume) as a reductant. 10 mg sample was used for each measurement. Before introducing to the H_2-Ar stream, the sample was pretreated in the N_2 stream at 200 °C for 1 h. The H_2 consumption profile was collected from room temperature to 800 °C at a rate of 10 °C/min.

Temperature-programmed desorption (TPD) was operated on a Nicolet IS10 FT-IR spectrometer equipped with a 2 m path-length gas cell (2 L volume). Catalysts were evaluated in a fixed-bed quartz reactor (5 mm internal diameter) operating with a steady-state flow. 100 mg sample was primarily pretreated by argon (100 mL/min) at 200 °C for 1 h, then it is cooled to 100 °C and exposed to 500 ppm NH_3/Ar, 500 ppm NO/Ar + 5% O_2/Ar, or 500 ppm NH_3/Ar + 500 ppm NO/Ar + 5% O_2 (100 mL/min with 5% H_2O) for 2 h. Thereafter, excessive physisorbed species was removed by purging with argon at 100 °C for 1 h. All TPD tests were carried out by increasing the temperature from 100 to 600 °C at a rate of 10 °C /min and an argon flow rate of 100 mL/min.

The transient experiment was carried out to investigate the reactivity property of surface nitrates. Catalysts were evaluated in a fixed-bed quartz reactor (5 mm internal diameter) operating with a steady-state flow. 100 mg sample was primarily pretreated by argon (100 mL/min) at 200 °C for 1 h, then it is cooled to 30 °C and exposed to 500 ppm NO/Ar, + 5% O_2/Ar (100 mL/min) for 1 h. Thereafter, excessive physisorbed species were removed by purging with argon at 30 °C for 1 h and then switched to 500 ppm NH_3/Ar for 1 h. A quadrupole mass spectrometer was employed to detect N_2 during the temperature-programmed from 30 °C to 100 °C with a ramping rate of 5 °C/min.

The diffuse reflectance infrared Fourier transformed spectra (DRIFTS) were collected on a Nicolet Nexus 5700 FT-IR spectrometer equipped with a highly sensitive mercury cadmium telluride detector cooled by liquid N_2 with a scanning number of 32 at a resolution of 4 cm^{-1}, and a diffuse reflectance reaction cell (HARRICK) equipped with a KBr window and a heater that allowed samples to be heated was used. The catalyst powder placed on a sample holder was carefully flattened to enhance the IR reflection. Before tests, the sample was pretreated in a flowing N_2 stream at 400 °C for 0.5 h to eliminate physisorbed water and other impurities. After cooling to the target temperature, the background was collected and the sample was exposed to a controlled stream of the specific atmosphere: 1000 ppm NH_3 and 1000 ppm NO + 5% O_2. All reaction gas above was balanced at a N_2 flow rate of 50 mL/min.

2.3. Activity measurement

The catalytic performances were evaluated in a fixed-bed quartz reactor with a 5 mm internal diameter under steady-state flow. The feed gas was 500 ppm NO, 500 ppm NH_3, 5% O_2, 5% H_2O (Ar in balance), and total gas flow was controlled at 100 mL/min. 100 mg catalyst was sieved to 40-60 mesh. Before tests, the catalyst was pretreated in a purified Ar stream at 200 °C for 30 min to avoid surface impurities. Then the mixed gases were switched on and activity data were collected at every target temperature after stabilizing for 30 min in the range of 50-250 °C. The concentration of effluent gases was analyzed on a Nicolet IS10 FT-IR spectrometer equipped with a 2 m path-length gas cell (2 L

volume). The NO conversion and N_2 selectivity were calculated based on the following equations:

$$\text{NO conversion}(\%) = \frac{C_{NO,\,in} - C_{NO,\,out}}{C_{NO,\,in}} \times 100\%$$

$$N_2 \text{ selectivity}(\%) = \frac{C_{NO,\,in} - C_{NO,\,out} + C_{NH_3,\,in} - C_{NH_3,\,out} - C_{NO_2,\,out} - 2C_{N_2O,\,out}}{C_{NO,\,in} - C_{NO,\,out} + C_{NH_3,\,in} - C_{NH_3,\,out}} \times 100\%$$

2.4. Kinetics measurement

Kinetics measurement was evaluated on the same equipment as activity tests. Catalysts were pretreated for 30 min at 200 °C under Ar flow to remove impurities. The stable state of NO conversion was controlled below 30% in an approximate kinetic regime. The feed gas was 100-500 ppm NO, 100-500 ppm NH_3, 5% O_2, 5% H_2O (Ar in balance), and total gas flow was controlled at 100 mL/min. In a typical measurement, 10 mg catalysts diluted with 90 mg inert SiC were pressed (60-80) and used, corresponding to a WHSV (weight hourly space velocity) of 600,000 $mL{\cdot}h^{-1}{\cdot}g^{-1}$. Activity evaluation was tested at 100 °C and the reaction rate (r) was calculated through the following equations:

$$r = \frac{v \times \alpha}{V_m}$$

where v represents the flow rate of NO ($m^3{\cdot}min^{-1}$), α is the NO conversion at a certain temperature (%), V_m is the gas molar constant ($m^3{\cdot}mol^{-1}$). To achieve viable kinetic data, the influences of internal and external diffusions are eliminated before the kinetic measurement, which is shown in Fig. S1 and Fig. S2.

3. Results and discussion

3.1. SCR performance and K resistance

Fig. 1 illustrates the NO conversion and N_2 selectivity of fresh/K-poisoned CeMn and hybrid catalysts from 50 to 250 °C under a weight hourly space velocity (WHSV) of 60,000 $mL{\cdot}h^{-1}{\cdot}g^{-1}$. Fresh CeMn reaches 100% NO conversion at 125 °C and maintains high activity within 125 and 175 °C, but the N_2 selectivity is quite unsatisfied and it drops to less than 80% at 125 °C (Fig. 1b). Contrastively, CeMn-Z5 yields 100% NO conversion within a much wider temperature window (100-250 °C) and higher N_2 selectivity (above 80% during 50-250 °C). What's more, original CeMn catalysts display disappointing resistance to K poisoning, and 0.5% (mass ratio) K_2O loading results in a 17% decrease of NO conversion at 100 °C. When increasing the loading to 2%, a drastic decline in NO conversion to less than 30% is observed (Fig. 1c). As a sharp comparison, the hybrid catalysts exhibit superior resistance to K toxicity. With the increase of K_2O loading from 0.5% to 2%, no obvious decrease in activity is exhibited and the catalyst can still acquire more than 97% NO conversion at 100 °C, demonstrating the indispensible role of ZSM-5 in increasing the resistance of CeMn to alkali metal poisoning.

By comparing with previous studies, it is worthy mentioning that the K resistance reported here is rather eye-catching. Fig. 2 gives a summary of the representative results over diverse catalysts reported in literatures (detailed test conditions are listed in Table S1) [2,4,6,9,12,19–29]. It can be seen that commercial V_2O_5-WO_3/TiO_2 suffers from a huge decrease of 90% in activity after the loading of 2% K_2O [2]. Cu-SSZ-13 fares better, but also acquires a decline of 12% in NO conversion with 1.7% K_2O loading [24]. Meanwhile, other catalysts reported to behave excellent K resistance also suffer from at least 5% loss in NO conversion when loaded with 0.25-2% K_2O. As such, it is safe to conclude that the hybrid catalyst obtained in this work shows remarkable performance in K resistance.

3.2. Structural and textural features

To approach the decisive reasons for the significant behavior of hybrid catalysts in K resistance, the structural and textural features are firstly studied. SEM and TEM are employed first to reveal the existing state of CeMn, ZSM-5, and hybrid catalysts, which are shown in Fig. 3 and Fig. S3. CeMn exhibits a smaller size, while cubic-like ZSM-5 is much larger and presented a particle size of about 500-600 nm. After mechanical grinding, the sizes of individual components keep almost the same and both small grains of CeMn and bulk ZSM-5 are observed. No significant breakage is observed for ZSM-5. As for the CeMn, only CeO_2 (1 1 1) lattice fringe of 0.31 nm is measured over CeMn catalyst and no lattice of Mn species is detected (Fig. 3c). The crystallinity of CeMn also does not experience significant change, indicating that mechanical grinding does not affect the catalyst structure.

The specific surface area of the obtained samples is registered in Table 1. CeMn exhibits a surface area (S_{BET}) of 133.5 m^2/g, and hybrid catalyst gets the value of 230.4 m^2/g, which approximates to the weighted average of independent components (ZSM-5 gets a specific area of 331.1 m^2/g). After K_2O loading, the change of S_{BET} displays different trend. For 2K/CeMn with the largest K, it only decreases by 2 m^2/g, indicating K is highly dispersed and the loss of activity can not be attributed to the change of surface area. Notably, for the hybrid catalysts, it undergoes a much evident change, as evidenced by 24 m^2/g in decrease for 2K/CeMn-Z5 sample. This can be reasonably attributed to K entering into the pore channel of ZSM-5 through acid-base coordination. Along with the capture of alkali metals by ZSM-5, the poisoning degree of CeMn is expected to be alleviated. And this may be one of the reasons why hybrid catalysts behave good resistance to K poisoning.

The crystal structure of fresh and K-poisoned catalysts is characterized by powder XRD, and results are shown in Fig. 4a. Fresh CeMn catalysts exhibit typical cubic fluorite structure with diffraction peaks at 2θ = 28.91, 33.48, 47.71, and 56.86° (ICDD-PDF#34-0394), and no peaks from MnO_x species are detected. As for hybrid catalysts, the emerged peaks ranged in 2θ = 20-25° (marked in red diamonds) are

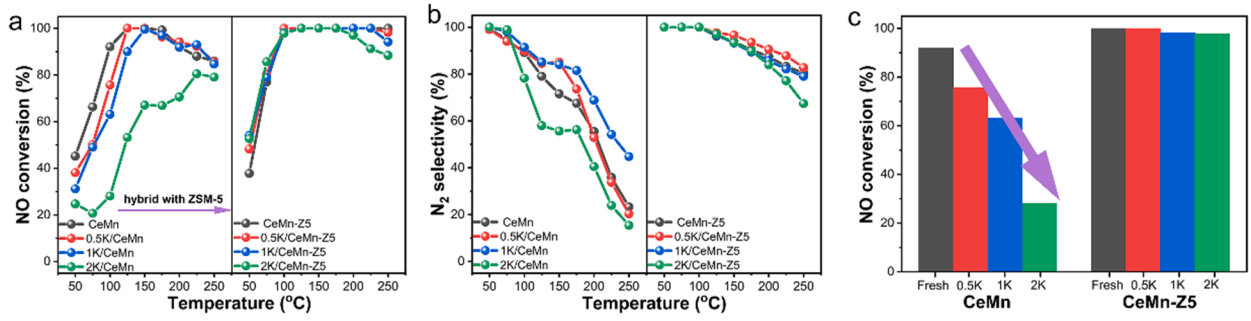

Fig. 1. (a) NO conversion and (b) N_2 selectivity over fresh/K-poisoned CeMn-based catalysts as a function of reaction temperature; (c) NO conversion versus K_2O loading at 100 °C over CeMn and CeMn-Z5. Reaction conditions: 500 ppm NO, 500 ppm NH_3, 5% O_2, 5% H_2O, and balanced with Ar, WHSV = 60,000 $mL{\cdot}h^{-1}{\cdot}g^{-1}$.

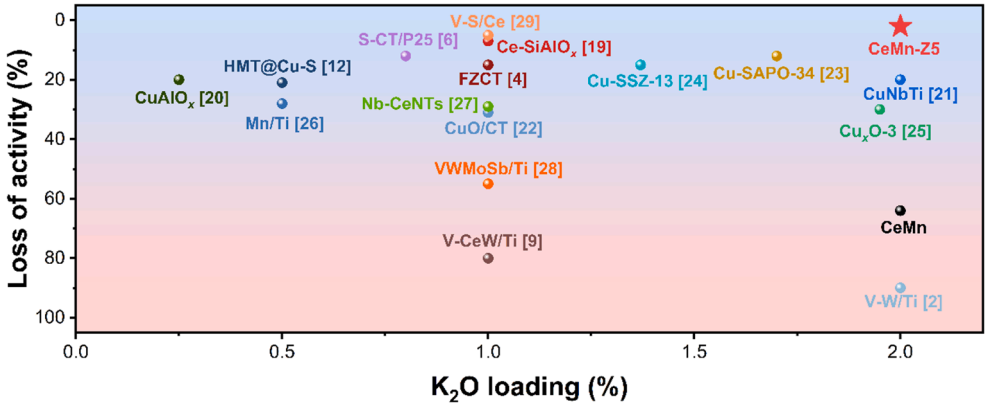

Fig. 2. Comparison of the anti-K performance of present work with literature reports (references are labeled in brackets).

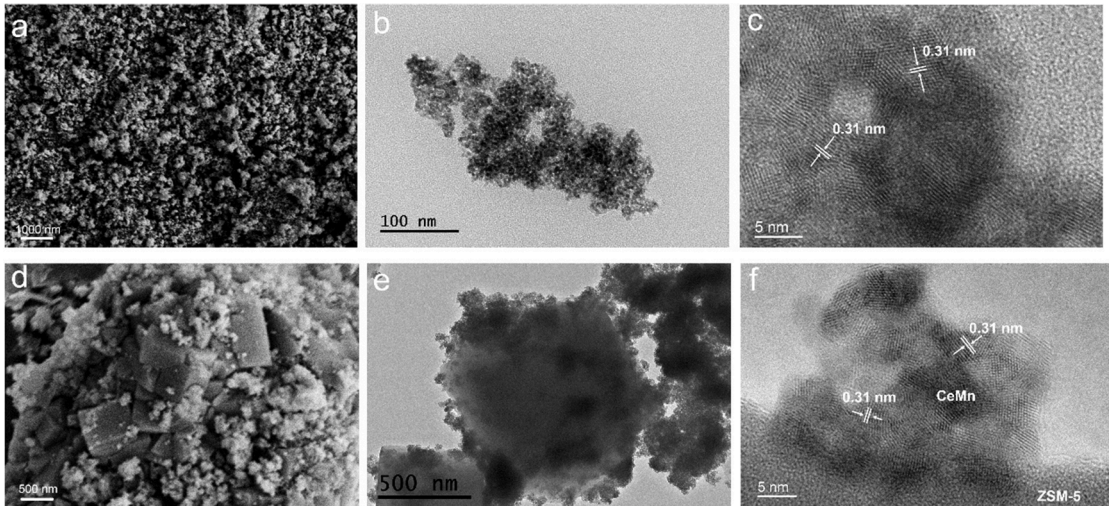

Fig. 3. SEM and TEM images of (a-c) CeMn and (d-f) CeMn-Z5.

Table 1
BET surface and the calculated ratio of Ce^{3+} over CeMn and hybrid catalysts from XPS results.

Sample	BET ($m^2 \cdot g^{-1}$)	$Ce^{3+}/(Ce^{3+}+Ce^{4+})$ (%)
CeMn	133.5	23.36
0.5K/CeMn	134.5	18.33
1K/CeMn	136.9	13.53
2K/CeMn	131.5	12.77
CeMn-Z5	230.4	23.51
0.5K/CeMn-Z5	231.7	19.87
1K/CeMn-Z5	220.7	15.64
2K/CeMn-Z5	206.3	13.76
ZSM-5	331.1	/

attributed to the diffraction peaks from ZSM-5. It has been previously reported that as a new method to prepare functional materials, mechanical grinding has the potential to reduce crystallite size [30]. As such, the major peaks of fresh CeMn and hybrid catalyst are compared and no peak broadening is observed (Fig. 4b). As for K-poisoned CeMn catalysts, the signal of K species is absent, indicating they are highly dispersed over CeMn. The diffraction peaks at 28.91° of poisoned hybrid catalysts are similar to that of original CeMn, while the intensity of peaks belonging to zeolites decreases with K_2O loading (Fig. 3c), in line with the result of K loaded ZSM-5 (Fig. S4) This conveys that K has an interaction with the ZSM-5 framework, which supports BET result.

XPS is further adopted to analyze the electronic structure. As shown in Fig. 4d-e, no obvious shift in the binding energy is detected for Ce *3d* between CeMn and CeMn-Z5, and quantitative calculation of $Ce^{3+}/(Ce^{3+}+Ce^{4+})$ ratio also shows no conspicuous change (23.36 *vs.* 23.51%, Table 1). This proves solid-state ion exchange does not occur during hybridization [31]. After 2% K_2O loading, the Ce^{3+} ratios of both CeMn and hybrid catalysts decrease. This indicates partial alkali metals are still located on the CeMn entity, although basically they can be captured by ZSM-5 through acid-base coordination.

Based on the discussion above, mechanical grinding do not change the structure of ZSM-5 and CeMn. And it is also not the change in structure and textural property that causes the catalytic deactivation of CeMn from K. In addition, even if some K are locates on CeMn component in the hybrid catalyst, no obvious deactivation is detected. To further explore the reason for the superior K resistance of hybrid catalysts, the redox and acid properties are investigated.

3.3. *Reduction behavior and acidic property*

H_2-TPR is employed to study the reduction behavior of fresh and poisoned catalysts and the corresponding results are shown in Fig. 5a-b. The peaks at 494 and 768 °C over original CeMn can be ascribed to the reduction of surface and bulk Ce species [32–33], while the peaks between 120 and 480 °C are related to the reduction of Mn species. Murugan *et al.* proposed that there mainly existed Mn^{3+} and Mn^{2+} in $Ce_{1-x}Mn_xO_{2-\delta}$ solid solutions [34]. Thus, the two peaks at 273 and 392 °C can be related to the reduction processes of $Mn_2O_3 \rightarrow Mn_3O_4$ and $Mn_3O_4 \rightarrow$

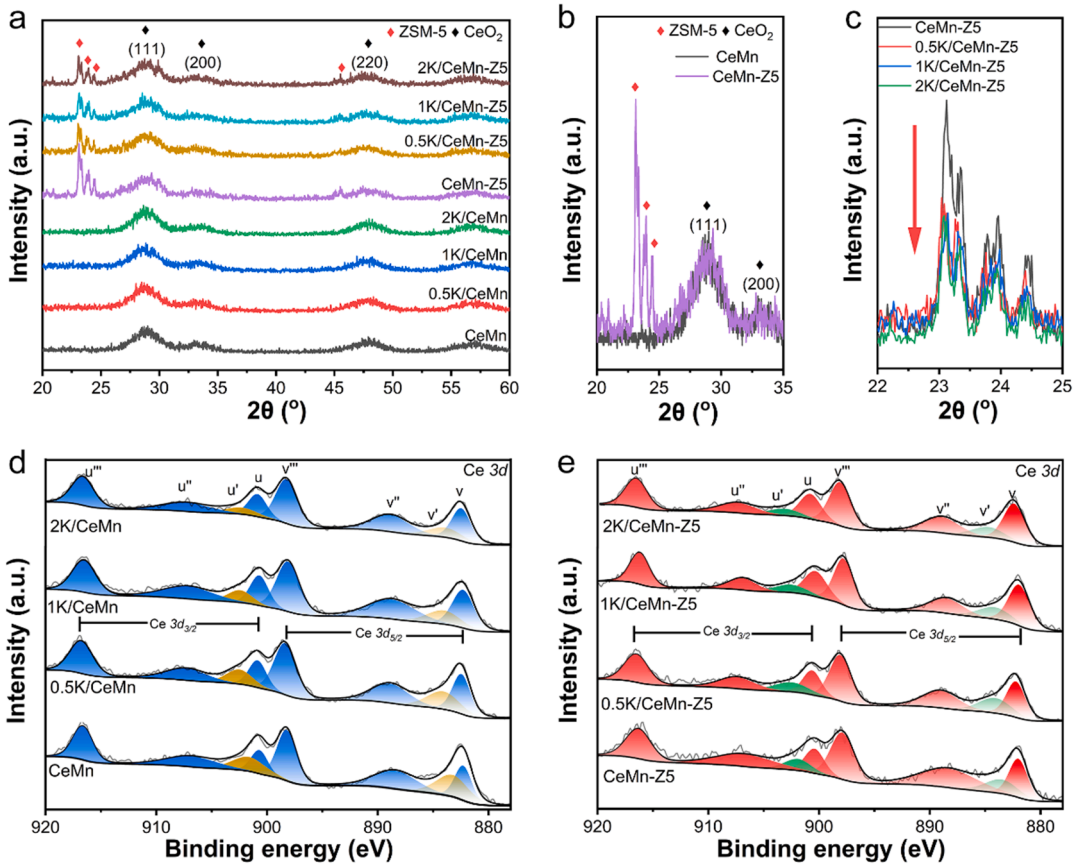

Fig. 4. The results of (a-c) XRD patterns and (d, e) Ce *3d* XPS spectra of fresh/K-poisoned CeMn and CeMn-Z5 catalysts.

MnO. Compared with original CeMn, the reduction peaks of fresh hybrid catalyst show no obvious variation, indicating the introduction of ZSM-5 through mechanical grinding does not exert significant influence on the redox property of CeMn.

As for K-poisoned catalysts, little changes can be observed over peaks belonging to Ce species, while the two peaks ascribed to Mn species shift to lower temperature direction obviously from 273 and 392 °C to 248 and 371 °C over 0.5K/CeMn. With further increase of K_2O loading, the reduction temperature turns higher slightly, but they are still lower than those over fresh CeMn. Besides, the H_2 consumption signal at low temperature becomes more obvious. These results are in line with the literature reports that suitable K_2O loading can increase the redox performance of Mn-based catalysts to some extent [35–37]. Compared with K-poisoned CeMn, the alteration on hybrid catalysts is much smaller, probably due to partial K being located on ZSM-5. Nevertheless, the decrease of reduction temperature and increase of Mn_2O_3 reduction amount at low temperature can be clearly observed for the 2% K_2O loaded sample, indicating a certain amount of K is located on CeMn.

It was previously reported the existence of alkali metals can interfere the adsorption of reactants, especially for NH_3, which inevitably inhibits the SCR activity. Therefore, we continue to explore the effect of K loading on the adsorption property of NH_3. All samples are pretreated under NH_3 stream at 100 °C for 120 min to ensure saturated adsorption. The obtained NH_3-TPD profiles and corresponding integrated results are presented in Fig. 5c-d and Table 2, respectively. CeMn presents only one desorption peak at low temperature. Quantitative analysis shows NH_3 adsorption over fresh CeMn is 0.14 mmol/g and this value decreases by only 25% after 2% K_2O loading, which can hardly explain the significant loss (nearly 70%) in activity. As for hybrid catalysts, the storage of NH_3 undergoes a significant increase to 1.19 mmol/g, almost 8.5 times the adsorption amount of original CeMn. Further inspection reveals that the introduction of ZSM-5 increases both weak and moderate NH_3 adsorption sites. This behavior can be well attributed to the existence of Lewis acid sites on Al sites (desorption peak at low temperature) and Brønsted acid sites of the zeolite skeleton (desorption peak at moderate temperature) [38–39]. And K loading on ZSM-5 can bring in the decline of both Lewis and Brønsted acid sites (Fig. S5). From Table 2, we know when 2% K_2O is loaded over hybrid catalysts, about 86% of acid sites are eliminated (from 1.19 mmol/g to 0.17 mmol/g). However, this exerts negligible influence on NO conversion, demonstrating the insignificant role of acid property in controlling K resistance.

3.4. Adsorption property of NO_x species and calculated K distribution

Since the redox property and NH_3 adsorption results obtained above give no clear evidence for the apparent difference in K resistance between CeMn and hybrid catalyst, we further focus on the impact of K loading on the adsorption and reactive properties of surface NO_x species. Previous studies have shown that diverse NO_x species are present on ceria-based catalysts when exposed to NO + O_2 stream. Among them, some are active and they can accelerate the reaction via the L-H mechanism, while others are rather inert and they stably occupy active sites resulting in deactivation of SCR catalysts [33,40]. Firstly, to approach the adsorption property of surface NO_x species and obtain their quantitative information, NO_x-TPD characterization after NO + O_2 adsorption is carried out and the result is shown in Fig. 6a-b and Table 2. Fresh CeMn shows remarkable NO and NO_2 desorption, and K loading exerts a significant influence. As can be seen in Table 2, the NO desorption increases with K loading from 0.49 to 0.88 mmol/g, while NO_2 desorption decreases from 0.47 to 0.06 mmol/g. K-loaded materials have been widely studied as alternatives for Ba-based NO_x storage materials (NSM) due to their remarkable ability to adsorb NO_x [41,42].

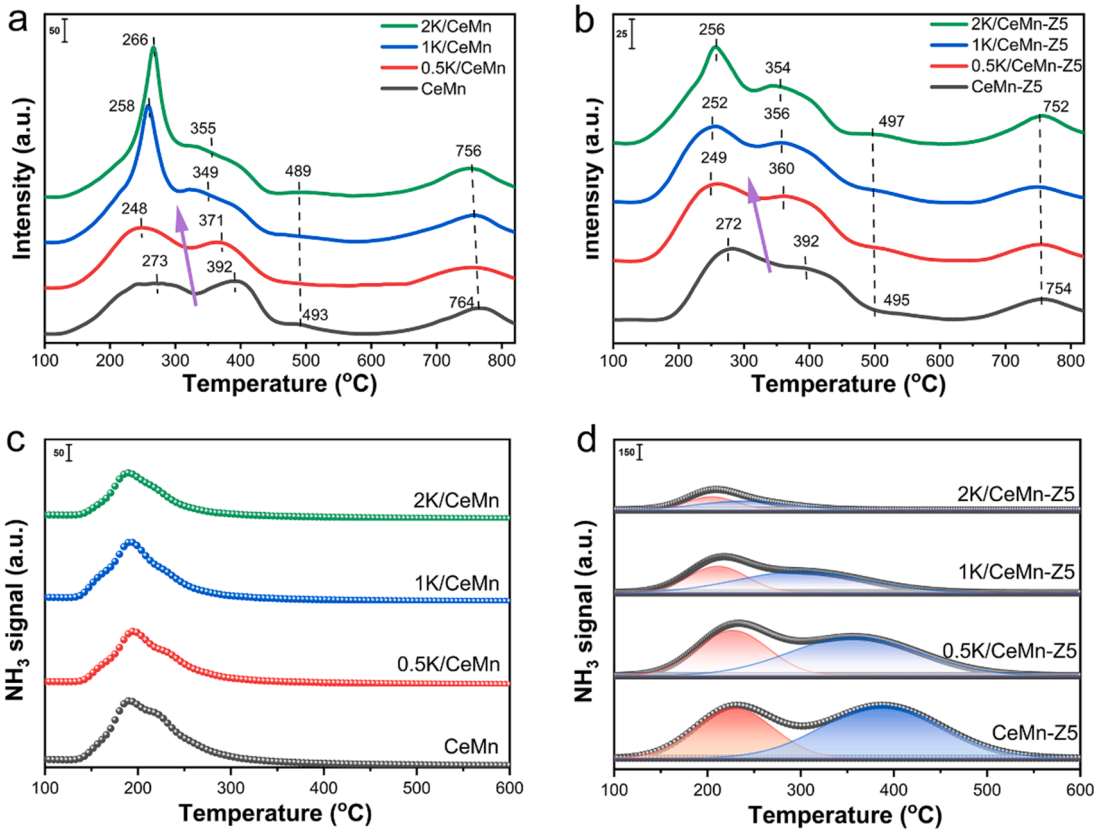

Fig. 5. H_2-TPR and NH_3-TPD profiles over fresh/K-poisoned (a, c) CeMn and (b, d) CeMn-Z5 samples.

Table 2
Quantitive result of NH_3-TPD and NO-TPD.

Sample	NH_3 (mmol·g^{-1})	NO (mmol·g^{-1})	NO_2 (mmol·g^{-1})
CeMn	0.14	0.49	0.47
0.5K/CeMn	0.12	0.68	0.19
1K/CeMn	0.12	0.76	0.08
2K/CeMn	0.10	0.88	0.06
CeMn-Z5	1.2	0.19	0.016
0.5K/CeMn-Z5	0.98	0.33	0.009
1K/CeMn-Z5	0.51	0.37	0.009
2K/CeMn-Z5	0.17	0.44	0.010

Based on the different evolutionary trends of NO and NO_2 desorption with increased K_2O loading, it is reasonable to speculate that the additional NO signal is from the new anchoring sites provided by K occupying on the original NO_2 desorption sites. As for CeMn-Z5, little NO_2 desorption can be observed, while the desorption signal of NO still increases from 0.19 to 0.44 mmol/g, verifying the general function of K_2O loading as additional NO_x adsorption sites.

Since both fresh ZSM-5 and 2K/ZSM-5 are unable to anchor NO and NO_2 (Fig. S6), the increase in NO_x adsorption over hybrid catalyst can be reasonably ascribed to the improved NO_x storage induced by K in contact with CeMn. It is also confirmed from Fig. 6a-b that the nitrates adsorbed over alkali metals desorb in form of NO, which prompts us to estimate the amount of K on CeMn according to the increase of NO desorption signals. Interestingly, there indeed exists a good linear relationship (R^2 = 0.998) between the increased NO adsorption and K loading over CeMn catalysts (Fig. 6c). The deposited K on CeMn entity in poisoned hybrid catalysts is thus obtained according to this relationship and the corresponding spatial distribution is shown in Fig. 6d. It shows that K preferentially enters ZSM-5 when the loading is as low as 0.5% over CeMn-Z5 (0.42% on ZSM-5 vs. 0.08% on MnCe). With K_2O loading rising, the distribution on CeMn gradually increases. Evidently, for the 2% K_2O loaded sample (2K/CeMn-Z5), about half K_2O (0.91% vs. 1.09%) is located on CeMn.

Information on the local distribution of K over 2K/CeMn-Z5 is further obtained with a TEM-EDS analysis and the result is shown in Fig. 7. CeMn and ZSM-5 exist separately, while K element appears to distribute evenly over both CeMn and ZSM-5, in line with the conclusion of NO-TPD. It has been shown in Fig. 1a that 1% K_2O loading on CeMn results in a great decrease of more than 30% in NO conversion. Thus, in addition to serving as sacrifice sites to alleviate CeMn catalysts poisoning, there must be other reasons for ZSM-5 to maintain the high activity of hybrid catalysts under high K loading toxicity.

3.5. *Reactive property of surface nitrates*

The result of NO_x-TPD after NO + O_2 adsorption reveals diverse NO_x species are present over CeMn catalysts and introduction of ZSM-5 or K can shape their distribution and desorption property. To further investigate the reactivity of these surface NO_x speices, a series of characterizations are operated. Fig. 8 shows the *in situ* DRIFTS results of NH_3 reaction with surface NO_x over various catalysts. Several signals belonging to bridging bidentate nitrates (1601 cm^{-1}), monodentate nitrates (1519 and 1270 cm^{-1}), chelating bidentate nitrates (1233 cm^{-1}), bridging monodentate nitrates (1573 cm^{-1}), and ionic nitrate (1351 cm^{-1}) are present on original CeMn after the adsorption of NO + O_2 [43,44]. After NH_3 exposure, the peaks belonging to diverse nitrates vanish quickly, and peaks centered at 1426 and 1351 cm^{-1} appear. These two peaks can be ascribed to free NO_3^- and NH_4^+, which indicates the existence of NH_4NO_3. NH_4NO_3 is widely reported to be an important intermediate in NH_3-SCR [45–46]. However, for 2K/CeMn (Fig. 8b), the peak at 1601 cm^{-1} disappears during NO + O_2 adsorption process, indicating the existence of K influences the types of surface nitrate species on CeMn. After exposure to NH_3, these peaks ascribed to nitrates

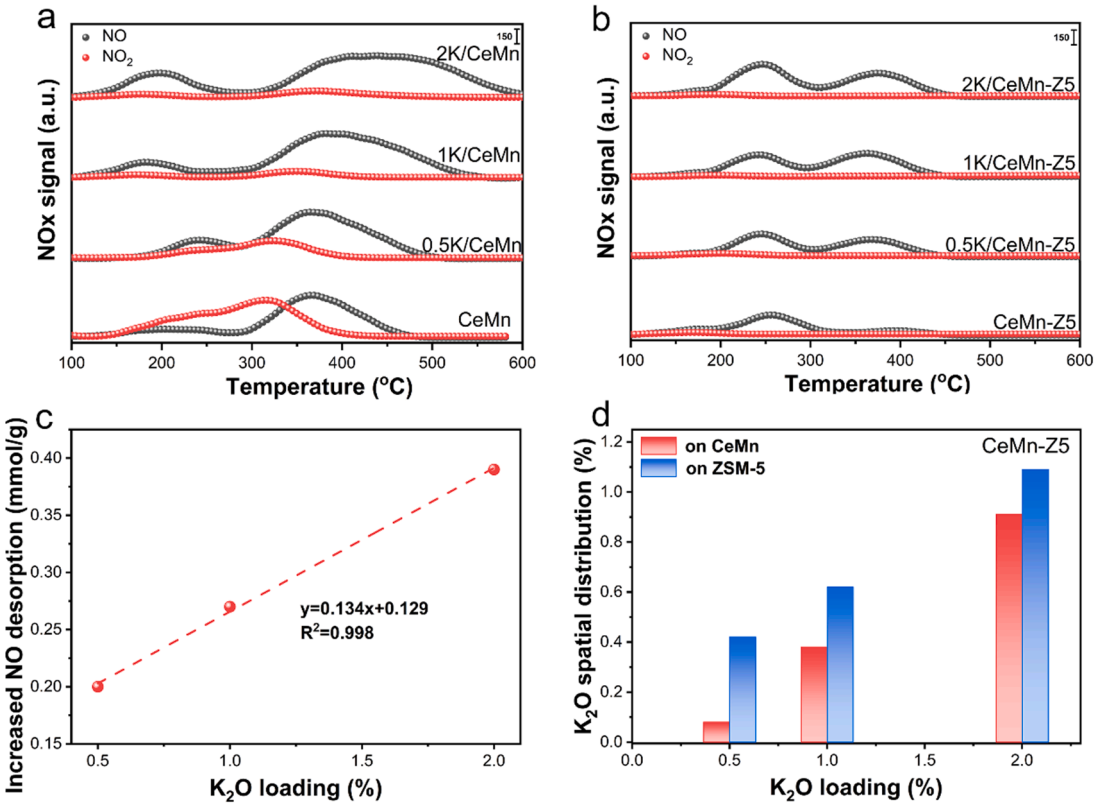

Fig. 6. NO_x-TPD patterns (following NO + O_2 adsorption) of fresh/2% K_2O poisoned (a) CeMn and (b) CeMn-Z5; (c) linear relationship between increased NO desorption and K loading over CeMn catalyst; (d) calculated K distribution over CeMn-Z5 via analysis of NO_x-TPD result.

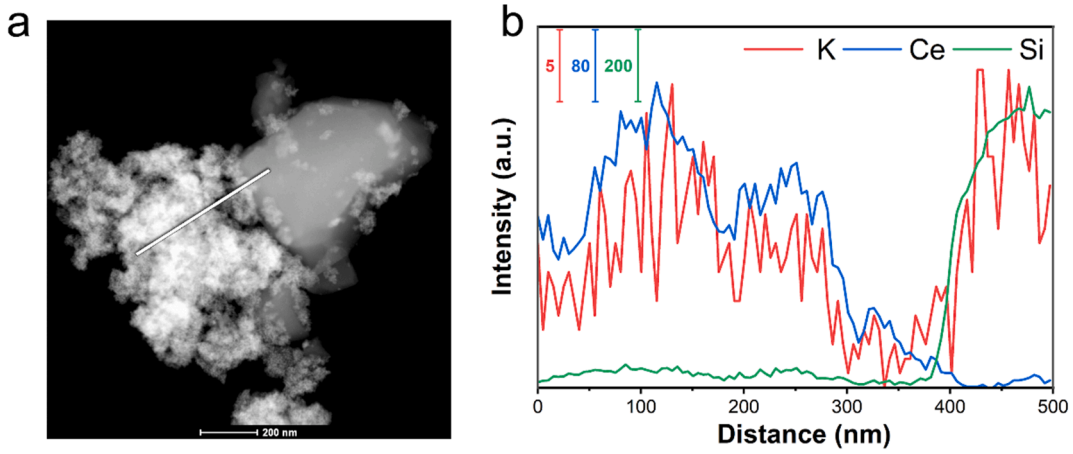

Fig. 7. (a) TEM image and (b) line-EDS of 2K/CeMn-Z5.

species show no significant changes and the signal of NH_4NO_3 (1426 and 1351 cm^{-1}) is absent. It suggests that the nitrates introduced by K loading are "inert" and not involved in the SCR process.

As for hybrid catalysts, the peaks belonging to bridging bidentate nitrates, monodentate nitrates, chelating bidentate nitrates, and bridging monodentate nitrates also emerge and can be quickly consumed by NH_3, no matter whether the catalysts are poisoned or not (Fig. 8c-d). This is also in line with the result of transient experiment (Fig. S7) that the nitrates introduced by K fail to participate in the reaction with NH_3, where N_2 signal can hardly be detected. However, the addition of ZSM-5 can obviously promote the reactivity of nitrates introduced by K poisoning. Amazingly, the poisoned catalysts even produce more N_2 compared with original hybrid catalysts, which may come from more nitrates introduced by K_2O poisoning (Table 2).

Kinetics measurement related to reaction orders of individual reactants is further employed to judge whether adsorbed species participate in the reaction and simultaneously explore the reaction mechanism. The stable state of NO conversion is controlled below 20% in an approximate kinetic regime and the influences of internal and external diffusions have been eliminated before the measurement, which are shown in Fig. S1 and Fig. S2. The rate of NO conversion can be described as $r_{NO} = k[NO]^{\alpha}[NH_3]^{\beta}[O_2]^{\gamma}$ with α, β, and λ being constants [3,47]. It is reported that the NH_3-SCR reaction acts as zero-order dependence with O_2 when the concentration surpasses 1% (5% O_2 under test conditions in this work) [48]. As such, only NO and NH_3 (α and β) reaction orders are taken into account and the result is shown in Fig. 9 ($R^2 > 0.95$). The NO

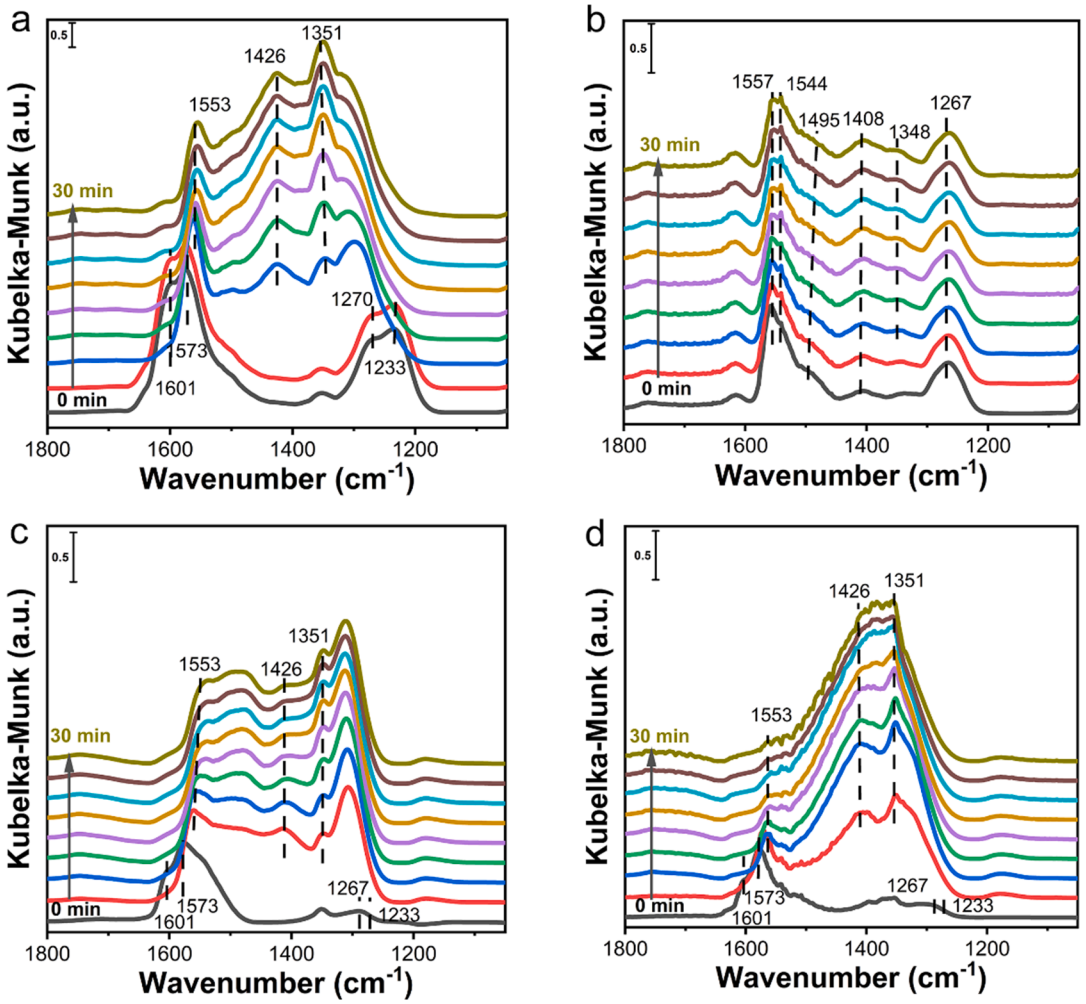

Fig. 8. *In situ* DRIFTS of the reaction between NH_3 and pre-adsorbed NO + O_2 at 100 °C over (a) CeMn, (b) 2K/CeMn, (c) CeMn-Z5, and (d) 2K/CeMn-Z5.

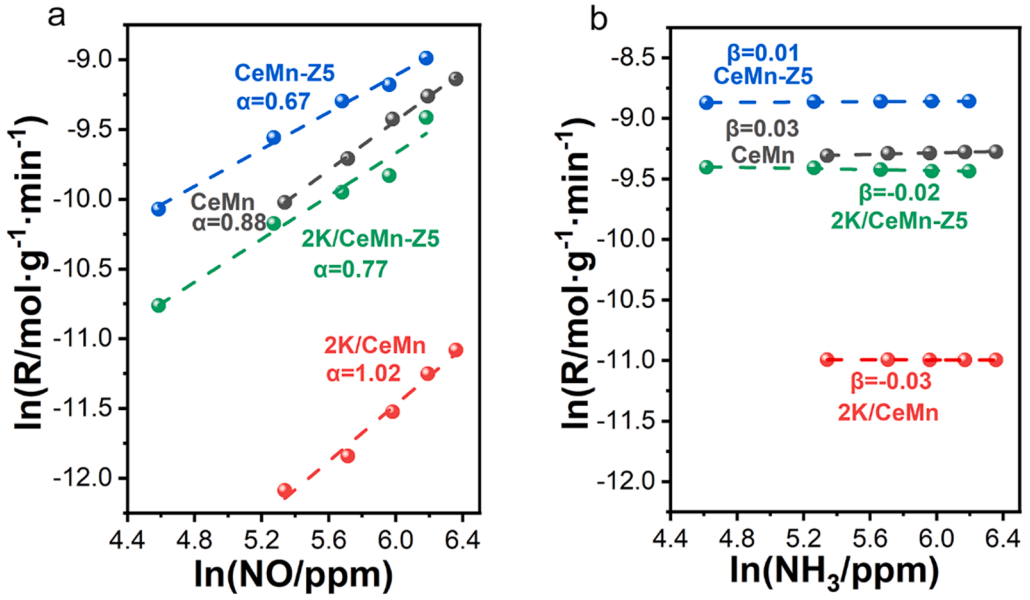

Fig. 9. Reaction order test result for (a) NO and (b) NH_3 of fresh/poisoned CeMn and corresponding hybrid catalyst at 100 °C.

reaction order is 0.88 for original CeMn, indicating that L-H and E-R mechanisms both contribute to the reaction. However, when 2% K_2O is loaded over CeMn, the α of poisoned catalysts experiences apparent change and the value is increased to 1.02, suggesting that L-H mechanism is cut off over poisoned catalysts and the reaction only follows E-R mechanism. As for hybrid catalysts, the α of fresh catalysts is 0.67, demonstrating that the introduction of ZSM-5 strengthens the L-H mechanism and promotes the reactivity of nitrates over CeMn. When compare with original hybrid catalysts, we find that the α of poisoned catalysts turns 0.77, which is still lower than 1. It indicates that the nitrate over K poisoned CeMn can also participate in the SCR reaction with the addition of ZSM-5.

For reaction order β, Xiang *et al.* proposed that the introduction of nitrate by alkali metals could react with gaseous NH_3 and their measured reaction order of NH_3 was 0.307 [49]. As for the reaction order of the catalysts in this work, it is all close to zero for all fresh/poisoned CeMn and hybrid catalysts, suggesting that NH_3 mainly participates in the SCR reaction as adsorbed ammonia species.

To discriminate the NO_x species consumed in reaction condition (active nitrates), the comparison of NO_x-TPD results from catalyst pretreated with NO + O_2 and the reaction atmosphere (NO + O_2 + NH_3) is conducted (Fig. 10). It is easy to understand that the integrated difference between NO_x desorption signals from respectively NO + O_2 and reaction atmosphere can reflect the amount of NO_x taking part in the reaction. As presented in Fig. 10a, only 0.01 mmol/g NO_2 desorbs over original CeMn pretreated by reaction gases, much less than the corresponding value (0.47 mmol/g) from NO + O_2 (Table 2). This indicates the sites related to NO_2 desorption are more active in reaction and it is occupied by alkali metals after poisoning. As for NO signal, its value is also decreased (from 0.49 mmol/g to 0.22 mmol/g), indicating L-H mechanism happens and nitrates are involved in the reaction. However, after 2% K_2O is introduced onto CeMn, no NO_2 desorption are detected and the amount of NO desorbed holds almost the same as that during NO + O_2 adsorption (0.86 mmol/g *vs.* 0.88 mmol/g). Combined with the results of *in situ* DRIFTS, tranient experiment, and kinetics analysis, clear evidence is shown that nitrates formed over K can hardly participate in the SCR reaction process and the L-H mechanism is largely cut off. The increased NO_x species resulting from K introduction is "inert", and this can give good explanation for the obvious CeMn poisoning caused by K loading.

As for hybrid catalysts, result (Fig. 10b) shows the preserved nitrate species are much fewer than fresh CeMn after the SCR reaction, verifying the addition of ZSM-5 can promote the participation of nitrates in the reaction. Moreover, there are only 0.09 mmol/g of NO desorbs from poisoned catalysts (versus 0.44 mmol/g pretreated by NO + O_2 stream), verifying addition of ZSM-5 can play the unique role in activating "inert nitrates" introduced by K.

3.6. K resistance mechanism over hybrid catalysts

To disclose more details about the promoted K-resistance mechanism with the addition of ZSM-5, a controlled catalyst is designed. That is, fresh ZSM-5 is mixed with CeMn pre-poisoned by 2% K_2O. Pure ZSM-5 has no SCR activity (Fig. S8). Thus, the study on this catalyst owns the distinct merit that it can directly reveal the effect of ZSM-5 on the transformation of surface inert species on poisoned CeMn catalyst, since in this case all of the K species are restricted on CeMn. We have known from NO_x-TPD (following NO + O_2 adsorption) result that K acts as the site for NO_x adsorption, which is excluded from SCR reaction and results in decreased activity. However, after mixing with ZSM-5, it is clearly shown (Fig. 11a) that the NO conversion of poisoned CeMn dramatically recovers from 25 to nearly 100%. Further quantitative results from NO_x-TPD following reaction atmosphere adsorption (Fig. 11b) show the deposited nitrate species under reaction atmosphere is greatly restrained and only 0.04 mmol/g NO desorbs from the surface of CeMn. This clearly verifies that deactivated catalysts resulting from the cut-off of L-H mechanism can be re-activated by simple mechanical grinding with ZSM-5, which provides an extremely facile and robust route in regenerating alkali metal poisoned catalysts.

To ascertain the origin of ZSM-5 coupling in promoting surface nitrates consumption on K poisoned CeMn, the NH_3-TPD profiles are recorded. From Fig. 12a, we can see that by comparing the signal difference in NH_3 desorption from sample pretreated with NH_3 and the reaction atmosphere, only 2.3% NH_3 is involved in the reaction for 2K/CeMn. After the introduction of ZSM-5, both acid sites at low temperature (0.27 mmol/g) and moderate temperature (0.12 mmol/g) increase. By referring to the signal from pure NH_3 adsorption, it is shown that under reaction atmosphere, the NH_3 adsorbed on Brønsted acid sites (desorb at moderate temperature) is mostly consumed and only 29% NH_3 at Lewis acid sites (desorb at weak temperature) is reduced, indicating that NH_3 from Brønsted acid sites may be more active in accelerating the reaction of alkali metal-added nitrates.

As a summary of the above characterization results, the corresponding reaction pathways over CeMn and hybrid catalysts are presented in Scheme 1. In contrast to disturbance of redox property and reduction of acid sites, the main reason for the CeMn deactivation from alkali metals is the formation of inert nitrates, which greatly restrain the L-H cycle of SCR reaction. After ZSM-5 coupling, the zeolite can naturally capture some of K species and acts as sacrifice sites, resulting in the alleviation of CeMn poisoning. More significantly, the formed inert nitrates over CeMn entity can be re-activated by the ammonia species introduced by ZSM-5, thus transforming NO_x adsorption sites from inert to active and ensuring the high resistance of hybrid catalysts to K.

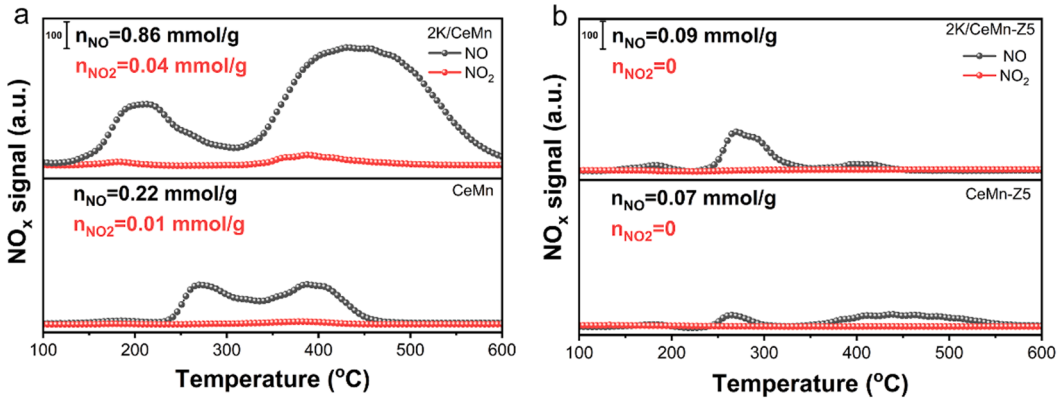

Fig. 10. NO_x-TPD patterns collected over fresh and 2% K_2O poisoned (a) CeMn and (b) CeMn-Z5 pretreated with reaction atmosphere (NO + O_2 + NH_3) at 100 °C.

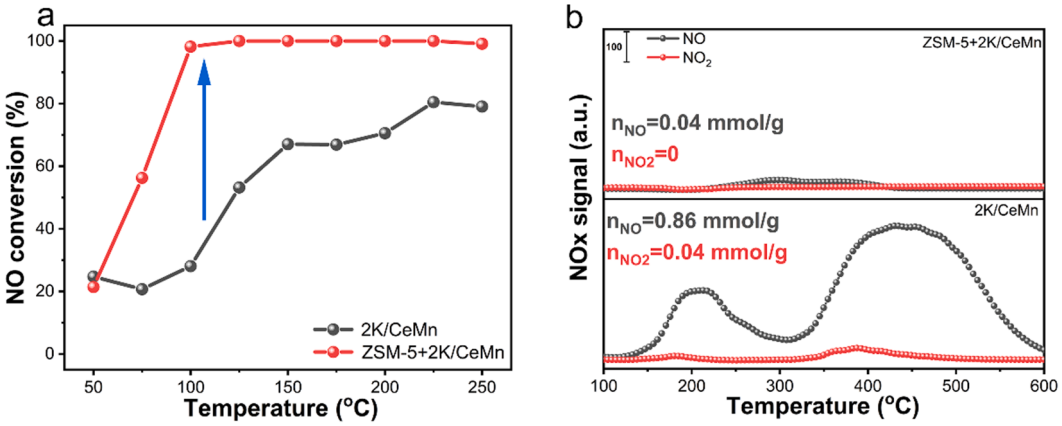

Fig. 11. The results of (a) NO conversion and (b) NO_x-TPD over 2K/CeMn and ZSM-5 + 2K/CeMn pretreated with reaction atmosphere and NO + O_2 adsorption. Reaction conditions: 500 ppm NO, 500 ppm NH_3, 5% O_2, 5% H_2O, and balanced with Ar, WHSV = 60,000 $mL{\cdot}h^{-1}{\cdot}g^{-1}$.

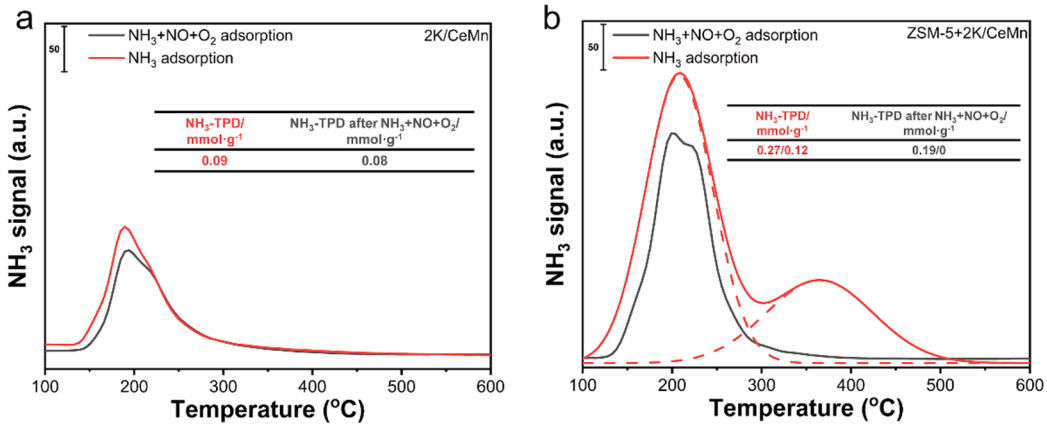

Fig. 12. The results of NH_3-TPD over (a) 2K/CeMn and (b) ZSM-5 + 2K/CeMn pretreated with reaction atmosphere and NH_3 adsorption.

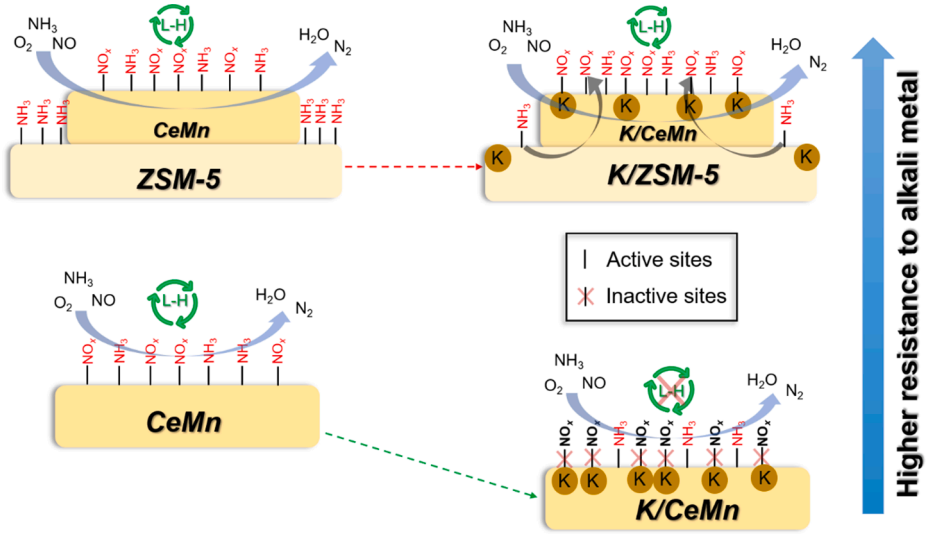

Scheme 1. Schematic illustration of the anti-K poisoning mechanism over CeMn catalyst coupled with ZSM-5.

4. Conclusion

In conclusion, a novel CeMn-Z5 hybrid catalysts prepared by facile mechanical grinding method was reported to exhibit excellent NH_3-SCR reaction property, especially the enhanced tolerance toward K, as compared with original CeMn catalysts. The loss of acid and redox property fails to explain the decrease in activity. Instead, the formation of inert nitrates introduced by alkali metals can be explained for deactivation, which cut off the L-H mechanism of SCR reaction. As for hybrid catalysts, the added ZSM-5 acts as sacrifice sites to capture some K based

on acid-base coordination interaction, leading to the alleviation of CeMn poisoning. More to the point, the inert nitrates formed over CeMn can be re-activated by ZSM-5, thus transforming inert sites to active sites and ensuring the high resistance of hybrid catalysts to alkali metals. And this method can also be employed in regenerating alkali metal poisoned catalysts. It is expected these results can inspire new sight in designing NH_3-SCR catalysts with excellent activity and poisoning tolerance for practical applications.

Declaration of Competing Interest

The authors declare that they have no known competing financial interests or personal relationships that could have appeared to influence the work reported in this paper.

Acknowledgements

The financial supports from the National Science Foundation of China (21976081, 21972062) and Major Scientific and Technological Project of Bingtuan (2018AA002), are greatly acknowledged.

Appendix A. Supplementary data

Information about detailed test conditions of anti-K catalysts reported in literature; elimination of internal and external diffusion; SEM and TEM images; XRD; NH_3-TPD; NO_x-TPD; transient experiment; NO conversion over ZSM-5. Supplementary data to this article can be found online at https://doi.org/10.1016/j.cej.2022.136530.

References

[1] Z. Lian, J. Wei, W. Shan, Y. Yu, P.M. Radjenovic, H. Zhang, G. He, F. Liu, J.F. Li, Z. Q. Tian, H. He, Adsorption-induced active vanadium species facilitate excellent performance in low-temperature catalytic NO_x abatement, J. Am. Chem. Soc. 143 (27) (2021) 10454–10461.

[2] L. Chen, J. Li, M. Ge, The poisoning effect of alkali metals doping over nano V_2O_5-WO_3/TiO_2 catalysts on selective catalytic reduction of NO_x by NH_3, Chem. Eng. J. 170 (2–3) (2011) 531–537.

[3] J.K. Lai, I.E. Wachs, A perspective on the selective catalytic reduction (SCR) of NO with NH_3 by supported V_2O_5-WO_3/TiO_2 catalysts, ACS Catal. 8 (7) (2018) 6537–6551.

[4] K. Kang, X. Yao, Y. Huang, J. Cao, J. Rong, W. Zhao, W. Luo, Y. Chen, Insights into the co-doping effect of Fe^{3+} and Zr^{4+} on the anti-K performance of $CeTiO_x$ catalyst for NH_3-SCR reaction, J. Hazard. Mater. 416 (2021), 125821.

[5] P. Hu, Z. Huang, X. Gu, F. Xu, J. Gao, Y. Wang, Y. Chen, X. Tang, Alkali-resistant mechanism of a hollandite $DeNO_x$ catalyst, Environ. Sci. Technol. 49 (11) (2015) 7042–7047.

[6] X. Yao, K. Kang, J. Cao, L. Chen, W. Luo, W. Zhao, J. Rong, Y. Chen, Enhancing the denitration performance and anti-K poisoning ability of CeO2-TiO2/P25 catalyst by H2SO4 pretreatment: structure-activity relationship and mechanism study, Appl. Catal., B 269 (2020).

[7] L. Han, S. Cai, M. Gao, J.Y. Hasegawa, P. Wang, J. Zhang, L. Shi, D. Zhang, Selective catalytic reduction of NO_x with NH_3 by using novel catalysts: State of the art and future prospects, Chem. Rev. 119 (19) (2019) 10916–10976.

[8] Y. Peng, J. Li, L. Chen, J. Chen, J. Han, H. Zhang, W. Han, Alkali metal poisoning of a CeO_2-WO_3 catalyst used in the selective catalytic reduction of NO_x with NH_3: an experimental and theoretical study, Environ. Sci. Technol. 46 (5) (2012) 2864–2869.

[9] Y. Peng, J. Li, W. Shi, J. Xu, J. Hao, Design strategies for development of SCR catalyst: improvement of alkali poisoning resistance and novel regeneration method, Environ. Sci. Technol. 46 (22) (2012) 12623–12629.

[10] S. Li, W. Huang, H. Xu, T. Chen, Y. Ke, Z. Qu, N. Yan, Alkali-induced deactivation mechanism of V_2O_5-WO_3/TiO_2 catalyst during selective catalytic reduction of NO by NH_3 in aluminum hydrate calcining flue gas. *Appl. Catal., B* **2020**, *270*, 118872.

[11] Z. Huang, X. Gu, W. Wen, P. Hu, M. Makkee, H. Lin, F. Kapteijn, X. Tang, A "smart" hollandite $DeNO_x$ catalyst: self-protection against alkali poisoning, Angew. Chem. Int. Ed. 52 (2) (2013) 660–664.

[12] K. Zha, L. Kang, C. Feng, L. Han, H. Li, T. Yan, P. Maitarad, L. Shi, D. Zhang, Improved NO_x reduction in the presence of alkali metals by using hollandite Mn-Ti oxide promoted Cu-SAPO-34 catalysts, Environ. Sci. Nano 5 (6) (2018) 1408–1419.

[13] Z. Fan, J.-W. Shi, C. Niu, B. Wang, C. He, Y. Cheng, The insight into the role of Al_2O_3 in promoting the SO_2 tolerance of MnO_x for low-temperature selective catalytic reduction of NO_x with NH_3, Chem. Eng. J. 398 (2020), 125572.

[14] H. Chang, X. Chen, J. Li, L. Ma, C. Wang, C. Liu, J.W. Schwank, J. Hao, Improvement of activity and SO_2 tolerance of Sn-modified MnO_x-CeO_2 catalysts for NH_3-SCR at low temperatures, Environ. Sci. Technol. 47 (10) (2013) 5294–5301.

[15] P.R. Ettireddy, N. Ettireddy, T. Boningari, R. Pardemann, P.G. Smirniotis, Investigation of the selective catalytic reduction of nitric oxide with ammonia over Mn/TiO_2 catalysts through transient isotopic labeling and in situ FT-IR studies, J. Catal. 292 (2012) 53–63.

[16] S.C. Xiong, J.J. Chen, N. Huang, T. Yan, Y. Peng, J.H. Li, The poisoning mechanism of gaseous HCl on low-temperature SCR catalysts: MnO_x-CeO_2 as an example, Appl. Catal., B 267 (2020), 118668.

[17] G.S. Qi, R.T. Yang, A superior catalyst for low-temperature NO reduction with NH_3, Chem. Commun. 7 (2003) 848–849.

[18] S. Xiong, J. Weng, Y. Liao, B. Li, S. Zou, Y. Geng, X. Xiao, N. Huang, S. Yang, Alkali metal deactivation on the low temperature selective catalytic reduction of NO_x with NH_3 over MnO_x-CeO_2: A mechanism study, J. Phys. Chem. C 120 (28) (2016) 15299–15309.

[19] L. Yan, Y. Ji, P. Wang, C. Feng, L. Han, H. Li, T. Yan, L. Shi, D. Zhang, Alkali and phosphorus resistant zeolite-like catalysts for NO_x reduction by NH_3, Environ. Sci. Technol. 54 (14) (2020) 9132–9141.

[20] Q. Yan, Y. Nie, R. Yang, Y. Cui, D. O'Hare, Q. Wang, Highly dispersed Cu_yAlO_x mixed oxides as superior low-temperature alkali metal and SO_2 resistant NH_3-SCR catalysts, Appl. Catal., A 538 (2017) 37–50.

[21] X. Wang, Q. Cong, L. Chen, Y. Shi, Y. Shi, S. Li, W. Li, The alkali resistance of CuNbTi catalyst for selective reduction of NO by NH_3: A comparative investigation with VWTi catalyst, Appl. Catal., B 246 (2019) 166–179.

[22] K. Kang, X. Yao, J. Cao, Z. Li, J. Rong, W. Luo, W. Zhao, Y. Chen, Enhancing the K resistance of $CeTiO_x$ catalyst in NH_3-SCR reaction by CuO modification, J. Hazard. Mater. 402 (2021), 123551.

[23] G. Yang, X. Du, J. Ran, X. Wang, Y. Chen, L. Zhang, V. Rac, V. Rakic, J. Crittenden, Irregular influence of alkali metals on Cu-SAPO-34 catalyst for selective catalytic reduction of NO_x with ammonia, J. Hazard. Mater. 387 (2020), 122007.

[24] C. Wang, W. Yan, Z. Wang, Z. Chen, J. Wang, J. Wang, J. Wang, M. Shen, X. Kang, The role of alkali metal ions on hydrothermal stability of Cu/SSZ-13 NH_3-SCR catalysts, Catal. Today 355 (2020) 482–492.

[25] Q. Wang, H. Xu, W. Huang, Z. Pan, H. Zhou, Metal organic frameworks-assisted fabrication of CuO/Cu_2O for enhanced selective catalytic reduction of NO_x by NH_3 at low temperatures, J. Hazard. Mater. 364 (2019) 499–508.

[26] L. Wei, Z. Wang, Y. Liu, G. Guo, H. Dai, S. Cui, J. Deng, Support promotion effect on the SO_2 and K^+ co-poisoning resistance of MnO_2/TiO_2 for NH_3-SCR of NO, J. Hazard. Mater. 416 (2021), 126117.

[27] P. Wang, S. Chen, S. Gao, J. Zhang, H. Wang, Z. Wu, Niobium oxide confined by ceria nanotubes as a novel SCR catalyst with excellent resistance to potassium, phosphorus, and lead, Appl. Catal., B 231 (2018) 299–309.

[28] P. Wu, K. Shen, Y. Liu, Y. Zhang, G. Li, H. Yang, S. Wang, Enhanced activity and alkali metal resistance in vanadium SCR catalyst via co-modification with Mo and Sb, Catal Sci. Technol. 11 (12) (2021) 4115–4132.

[29] G. Zhou, P. Maitarad, P. Wang, L. Han, T. Yan, H. Li, J. Zhang, L. Shi, D. Zhang, Alkali-resistant NO_x reduction over SCR catalysts via boosting NH_3 adsorption rates by in situ constructing the sacrificed sites, Environ. Sci. Technol. 54 (20) (2020) 13314–13321.

[30] W. Xu, X.C. Liu, K. Lu, Strain-induced microstructure refinement in pure Al below 100 nm in size, Acta Mater. 152 (2018) 138–147.

[31] M. Salazar, R. Becker, W. Grünert, Hybrid catalysts-an innovative route to improve catalyst performance in the selective catalytic reduction of NO by NH_3, Appl. Catal. B 165 (2015) 316–327.

[32] L. Zhang, W. Zou, K. Ma, Y. Cao, Y. Xiong, S. Wu, C. Tang, F. Gao, L. Dong, Sulfated temperature effects on the catalytic activity of CeO_2 in NH_3-selective catalytic reduction conditions, J. Phys. Chem. C 119 (2) (2015) 1155–1163.

[33] J. Ji, M. Jing, X. Wang, W. Tan, K. Guo, L. Li, X. Wang, W. Song, L. Cheng, J. Sun, W. Song, C. Tang, J. Liu, L. Dong, Activating low-temperature NH_3-SCR catalyst by breaking the strong interface between acid and redox sites: A case of model $Ce_2(SO_4)_3$-CeO_2 study, J. Catal. 399 (2021) 212–223.

[34] B. Murugan, A.V. Ramaswamy, D. Srinivas, C.S. Gopinath, V. Ramaswamy, Nature of manganese species in $Ce_{1-x}Mn_xO_{2-\delta}$ solid solutions synthesized by the solution combustion route, Chem. Mater. 17 (15) (2005) 3983–3993.

[35] X. Xie, Q. Tang, J. Zhang, J. Wang, P. Zhao, Y. Wang, M.B. Sullivan, Y. Yang, Effects of K-dopant on structure and activity of KMn/Al_2O_3 catalysts for CO oxidation: Experimental evidence and DFT calculation, Appl. Catal., A 520 (2016) 132–139.

[36] P. Zhao, N. Feng, F. Fang, H. Wan, G. Guan, Surface acid etching for efficient anchoring of potassium on 3DOM $La_{0.8}Sr_{0.2}MnO_3$ catalyst: An integration strategy for boosting soot and NO_x simultaneous elimination, J. Hazard. Mater. 409 (2021), 124916.

[37] K. Jirátová, J. Mikulová, J. Klempa, T. Grygar, Z. Bastl, F. Kovanda, Modification of Co-Mn-Al mixed oxide with potassium and its effect on deep oxidation of VOC, Appl. Catal., A 361 (1–2) (2009) 106–116.

[38] J.R. Anderson, K. Foger, T. Mole, R.A. Rajadhyaksha, J.V. Sanders, Reactions on ZSM-5-type zeolite catalysts, J. Catal. 58 (1) (1979) 114–130.

[39] N. Usberti, F. Gramigni, N.D. Nasello, U. Iacobone, T. Selleri, W. Hu, S. Liu, X. Gao, I. Nova, E. Tronconi, An experimental and modelling study of the reactivity of adsorbed NH_3 in the low temperature NH_3-SCR reduction half-cycle over a Cu-CHA catalyst, Appl. Catal., B 279 (2020) 119397.

[40] R. Zhang, W. Yang, N. Luo, P. Li, Z. Lei, B. Chen, Low-temperature NH_3-SCR of NO by lanthanum manganite perovskites: Effect of A-/B-site substitution and TiO_2/CeO_2 support, Appl. Catal., B 146 (2014) 94–104.

[41] H.P. Nguyen, S. Palma Del Valle, O. Marie, NO adsorption on K and Ba loaded on zirconia-titania NSR catalysts: A comparative study by in situ and operando IR spectroscopy, Appl. Catal., B 231 (2018) 391–399.

[42] T.J. Toops, D.B. Smith, W.P. Partridge, Quantification of the in situ DRIFT spectra of Pt/K/γ-A1$_2$O$_3$ NO$_x$ adsorber catalysts, Appl. Catal., B 58 (3–4) (2005) 245–254.
[43] W. Tan, J. Wang, L. Li, A. Liu, G. Song, K. Guo, Y. Luo, F. Liu, F. Gao, L. Dong, Gas phase sulfation of ceria-zirconia solid solutions for generating highly efficient and SO$_2$ resistant NH$_3$-SCR catalysts for NO removal, J. Hazard. Mater. 388 (2020), 121729.
[44] S. Yang, Y. Guo, H. Chang, L. Ma, Y. Peng, Z. Qu, N. Yan, C. Wang, J. Li, Novel effect of SO$_2$ on the SCR reaction over CeO$_2$: mechanism and significance, Appl. Catal., B 136–137 (2013) 19–28.
[45] X. Zhu, L. Zhang, Y. Dong, C. Ma, NO$_2$-NH$_3$ SCR over activated carbon: A combination of NH$_4$NO$_3$ formation and consumption, Energy Fuels 35 (7) (2021) 6167–6178.
[46] H. Kubota, C. Liu, T. Toyao, Z. Maeno, M. Ogura, N. Nakazawa, S. Inagaki, Y. Kubota, K.-I. Shimizu, Formation and reactions of NH$_4$NO$_3$ during transient and steady-state NH$_3$-SCR of NO$_x$ over H-AFX zeolites: spectroscopic and theoretical studies, ACS Catal. 10 (3) (2020) 2334–2344.
[47] Ma, S.; Zhao, X.; Li, Y.; Zhang, T.; Yuan, F.; Niu, X.; Zhu, Y., Effect of W on the acidity and redox performance of the Cu$_{0.02}$Fe$_{0.2}$W$_\alpha$TiO$_x$ (α = 0.01, 0.02, 0.03) catalysts for NH$_3$-SCR of NO. *Appl. Catal., B* **2019,** *248*, 226–238.
[48] G. Busca, L. Lietti, G. Ramis, F. Berti, Chemical and mechanistic aspects of the selective catalytic reduction of NO$_x$ by ammonia over oxide catalysts: A review, Appl. Catal., B 18 (1–2) (1998) 1–36.
[49] J. Xiang, X. Du, Y. Wan, Y. Chen, J. Ran, L. Zhang, Alkali-driven active site shift of fast SCR with NH$_3$ on V$_2$O$_5$-WO$_3$/TiO$_2$ catalyst via a novel Eley-Rideal mechanism, Catal. Sci. Technol. 9 (21) (2019) 6085–6091.